

# On-Chip Sensor for Simultaneous Temperature and Refractive Index Measurements Based on a Dual-Passband Microwave Photonic Filter

Jingxuan Liu, Hong Deng, *Student Member, IEEE*, Weifeng Zhang, *Student Member, IEEE*, and Jianping Yao , *Fellow, IEEE, Fellow, OSA*

**Abstract**—We propose and experimentally demonstrate an on-chip optical sensor based on a dual-passband microwave photonic filter (MPF) incorporating a silicon photonic integrated microdisk resonator (MDR). Two whispering gallery modes supported by the MDR that are experiencing different wavelength shifts are employed for simultaneous temperature and refractive index (RI) measurements. To increase the interrogation speed and resolution, the MDR is incorporated in an MPF to produce two microwave passbands. By applying a broadband linearly chirped microwave waveform to the MPF, two filtered microwave waveforms with their temporal locations or equivalently central frequencies corresponding to the wavelength shifts of the notches are generated. The measurement of the temporal locations or equivalently the central frequencies is performed at high speed and high resolution using a digital signal processor. To increase the signal-to-noise ratio of the filtered microwave waveforms, a noise reduction algorithm based on phase-only filtering is proposed and employed. The on-chip optical sensing system is experimentally demonstrated. The sensing system can provide high temperature and RI interrogation resolutions of  $2.4 \times 10^{-5}$  °C and  $9.1 \times 10^{-8}$  RIU at a high interrogation speed of 1 MHz.

**Index Terms**—Micro-disk resonator, microwave photonics, sensors, silicon photonics, refractive index, temperature.

## I. INTRODUCTION

**I**N THE past few decades, fiber Bragg grating (FBG) sensors have been extensively studied and employed for various applications thanks to the key advantages such as low cost, light weight, high sensitivity, resistance to harsh environment,

immunity to electromagnetic interference (EMI), and wavelength multiplexing capability. The fundamental principle behind the use of an FBG for optical sensing is its wavelength sensitivity to environmental changes, such as temperature and strain [1]. However, an FBG is not sensitive to refractive index (RI) change of the external medium surrounding the FBG, hence it cannot be directly employed as an RI sensor, or special design has to be made to increase its sensitivity to external RI changes by increasing the evanescent field interaction with the surrounding medium. Those special FBGs include a thinned FBG [2], a micro structured FBG [3], an etch-eroded FBG [4] and a microfiber-based FBG [5]. For all those special FBGs, the fiber diameters are significantly reduced, the durability and practicability of the sensors become low.

Silicon photonic devices implemented on a silicon-on-insulator (SOI) platform have a high potential for optical sensing owing to their high sensitivity to RI changes, which is extremely important for chemical diagnostics and label-free biosensing since the presence of molecules can be detected through measuring the RI changes [6]. A few types of SOI sensors, such as nanocavity sensors [7], micro-ring resonator sensors [8], micro-disk resonator sensors [9], and Bragg grating sensors [10], have been proposed. However, the sensing information encoded in these sensors is obtained through direct wavelength shift measurement, which is usually done by an optical spectrum analyzer (OSA). Due to the relatively poor resolution and low interrogation speed of an OSA, the performance of the sensors including sensing speed and resolution is poor. For many applications, however, high-speed and high-resolution interrogation is demanded, such as chemical and biological reaction detection.

Microwave photonics (MWP), an interdisciplinary field that encompasses optical, microwave, and electrical engineering, provides an effective solution to high-speed and high-resolution interrogation. The basic concept of achieving high-performance interrogation is to translate a wavelength variation in the optical domain to a microwave frequency change in the microwave domain, which can be real-time monitored by a digital signal processor (DSP) at a high speed and high resolution [11]. Various MWP-based interrogation solutions have recently been proposed and demonstrated. In [12], Fu *et al.* reported a high-frequency FBG interrogation system for strain sensing based on fiber Sagnac-loop-based microwave photonic filtering. The

Manuscript received April 17, 2018; revised June 30, 2018; accepted July 13, 2018. Date of publication July 17, 2018; date of current version August 8, 2018. This work was supported by the Natural Sciences and Engineering Research Council of Canada. The work of J. Liu was supported by the China Scholarship Council under a scholarship. (*Corresponding author: Jianping Yao.*)

J. Liu is with the Microwave Photonics Research Laboratory, School of Electrical Engineering and Computer Science, University of Ottawa, Ottawa, ON K1N 6N5, Canada, and also with the Key Laboratory of All Optical Network and Advanced Telecommunication Network, Ministry of Education, Institute of Lightwave Technology, Beijing Jiaotong University, Beijing 100044, China (e-mail: jliu333@uottawa.ca).

H. Deng, W. Zhang, and J. Yao are with the Microwave Photonics Research Laboratory, School of Electrical Engineering and Computer Science, University of Ottawa, Ottawa, ON K1N 6N5, Canada (e-mail: hdeng095@uottawa.ca; wzhan088@uottawa.ca; jpyao@uottawa.ca).

Color versions of one or more of the figures in this paper are available online at <http://ieeexplore.ieee.org>.

Digital Object Identifier 10.1109/JLT.2018.2856868

wavelength shift induced by a strain was converted into intensity variation of a recovered electronic microwave signal. Since the measurement was done in the electrical domain, the interrogation speed was increased. In [13], Liu *et al.* proposed a strain sensor based on a linearly chirped fiber Bragg grating (LCFBG) which was used to encode the sensing information in its spectral response. After spectral shaping and wavelength-to-time (SS-WTT) mapping [14], a linearly chirped microwave waveform (LCMW) was generated. The interrogation resolution was improved by correlating the generated chirped waveform with a chirped reference waveform to achieve pulse compression in a DSP. Since the approaches in [12], [13] cannot distinguish temperature and strain, the strain measurement accuracy is deteriorated due to temperature variations. To overcome the problem, in [15], Kong *et al.* demonstrated a thermal-insensitive transverse load sensor based on a dual-frequency optoelectronic oscillator (OEO) using a phase-shifted fiber Bragg grating (PS-FBG), which is employed as an oscillation frequency selection filter as well as a sensing element. Since the two frequencies from the OEO will have the same frequency shifts due to temperature change, the beating between the two frequencies will generate a third frequency which is not sensitive to temperature change, thus the impact due to temperature variations is eliminated for strain measurement. The temperature itself, however, cannot be measured. In addition, due to the gain competition between the two microwave frequencies in the OEO, the stability of the dual-frequency OEO is poor which would make the sensing accuracy reduced. Recently, we have proposed and demonstrated an optical sensor employing a micro-disk resonator (MDR) for temperature or RI sensing with high-speed and high-resolution interrogation [16]. However, the cross-sensitivity due to temperature and RI still exists.

In this paper, an on-chip optical sensor for simultaneous temperature and RI sensing based on a dual-passband microwave photonic filter (MPF) incorporating a silicon photonic integrated MDR is presented. Two whispering gallery modes (WGMs) supported by the MDR that are experiencing different wavelength shifts are employed. To increase the interrogation speed and resolution, the MDR is incorporated in an MPF to produce two microwave passbands. The MPF is implemented based on phase modulation and phase-modulation to intensity-modulation (PM-IM) conversion, to translate the spectral response of the two notches in the optical domain to two passbands in the microwave domain [17]. When the MDR experiences temperature and/or RI variations, the wavelengths of the two notches will shift, leading to the change in the central frequencies of the two microwave passbands. By applying a broadband LCMW to the MPF, two filtered microwave waveforms with their temporal locations or equivalently central frequencies corresponding to the wavelength shifts are generated. The measurement of the temporal locations or equivalently central frequencies is performed using a DSP at a high speed and high resolution. To increase the signal-to-noise ratio (SNR) of the filtered microwave waveforms, a noise reduction algorithm based on phase-only filtering is proposed and employed. The proposed approach is experimentally demonstrated. The measurement results show that interrogation resolutions for temperature and RI

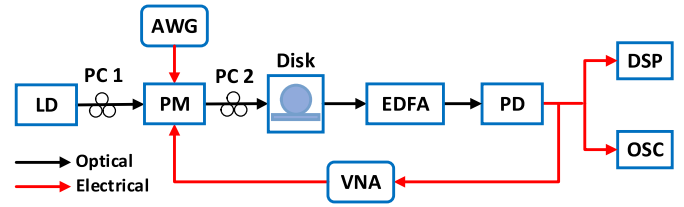


Fig. 1. Configuration of the proposed sensing system. LD, laser diode; PC, polarization controller; PM, phase modulator; AWG, arbitrary waveform generator; EDFA, erbium-doped fiber amplifier; PD, photodetector; VNA, vector network analyzer; DSP, digital signal processor; OSC, oscilloscope.

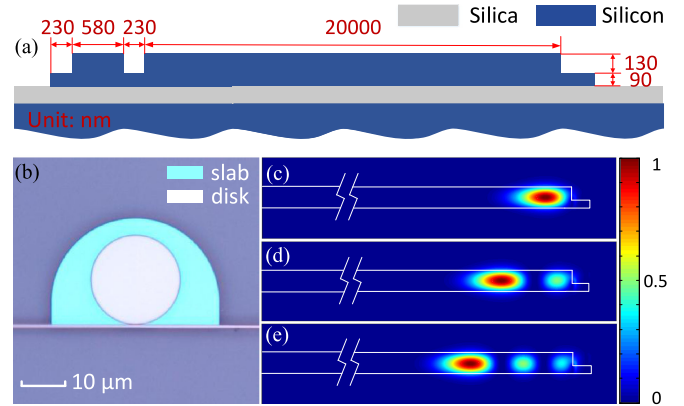


Fig. 2. (a) Cross-sectional view of the MDR, (b) the photomicrograph of the fabricated MDR and the mode field distributions of the (c) first-order (d) second-order (e) third-order radial TE mode in the MDR.

of  $2.4 \times 10^{-5} \text{ }^\circ\text{C}$  and  $9.1 \times 10^{-8} \text{ RIU}$ , respectively, at a speed of 1 MHz are achieved.

## II. PRINCIPLE

The schematic diagram of the proposed sensor employing an integrated silicon photonic MDR in a dual-passband MPF is shown in Fig. 1. The system consists of a laser diode (LD), a 40-GHz phase modulator (PM), an MDR, an erbium-doped optical amplifier (EDFA), a 45-GHz photodetector (PD), and a DSP. The joint operation of the LD, the PM, the MDR, and the PD corresponds to a dual-passband MPF, with the two passbands determined by the two notches of the MDR, realized based on phase modulation and PM-IM conversion [17]. A detailed discussion of the implementation of a dual-passband MPF can be found from [17]. In the proposed system, a broadband LCMW is applied to the dual-passband MPF. Two filtered microwave waveforms with their temporal locations or equivalently central frequencies representing the wavelength shifts of the two notches of the MDR are obtained. By measuring the temporal locations or equivalently central frequencies, the sensing information is retrieved.

The key component in the proposed sensing system is the integrated silicon photonic MDR, which should have a high Q factor to make the two microwave passbands have narrow bandwidths. To do so, the MDR is designed to have an additional slab waveguide to wrap the disk and the bus waveguide, to reduce the impact of the sidewall roughness [18]. Fig. 2(a) gives the cross-sectional view of an MDR. The disk has a diameter of  $20 \text{ } \mu\text{m}$  and

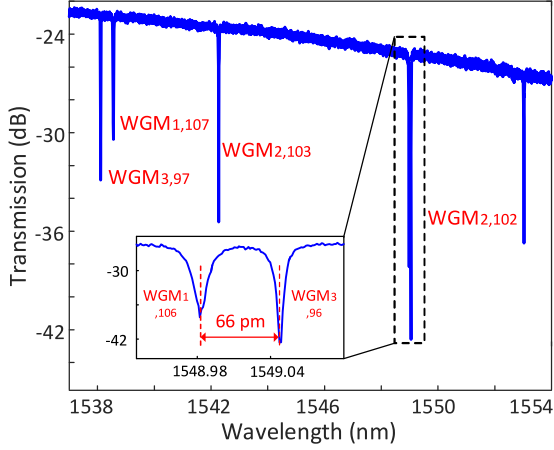


Fig. 3. Measured transmission spectrum of the MDR which can support three WGMs.

a height of 130 nm. The bus waveguide has a width of 580 nm and the height is kept identical to the height of the disk. The coupling gap between the disk and the bus waveguide is chosen to be 230 nm. The slab waveguide has a height of 90 nm. Fig. 2(b) shows the photomicrograph of the MDR comprising the disk, the slab waveguide and the bus waveguide. Fig. 2(c)–(e) shows the first-, second- and third-order radial TE WGMs supported by the MDR.

The transmission spectrum of the MDR is shown in Fig. 3. Each notch represents a specific  $WGM_{p,q}$  mode, where  $p$  and  $q$  are the numbers of radial and azimuthal harmonic orders, respectively. The first three orders of the WGMs are exited and the inset shows the zoom-in view of two modes,  $WGM_{1,106}$  and  $WGM_{3,96}$ . The  $WGM_{1,106}$  and  $WGM_{3,96}$  modes have 3-dB bandwidths of 20 pm and 15 pm, corresponding to Q factors of 77,000 and 100,000, respectively. The use of an MDR with a higher Q factor is of help in strengthening the interaction between the confined optical field and the outer environment changes including temperature and RI variations, which would lead to higher temperature and RI detection sensitivities. The two modes are used as two notches to produce two microwave passbands. The central wavelength difference between the two modes is 66 pm, corresponding to a frequency difference of 8.25 GHz.

By incorporating the MDR into an MPF, a dual-passband MPF is implemented. The operation principle of the dual-passband MPF is shown in Fig. 4. A phase-modulated double sideband with carrier (DSB+C) signal is applied to the MDR and the output signal is applied to a PD. If the optical carrier and the two sidebands are fully transmitted, the beating between the upper sideband and the optical carrier will cancel the beating between the lower sideband and the optical carrier, thus no microwave signal is generated except a direct current. When one sideband is filtered out by a notch, PM-IM conversion is realized, and a microwave signal is generated at the PD [17], [19]. In the proposed sensing system, the first-order sideband is filtered by two notches at two different frequencies, which leads to a dual-passband MPF. The central frequencies of the two

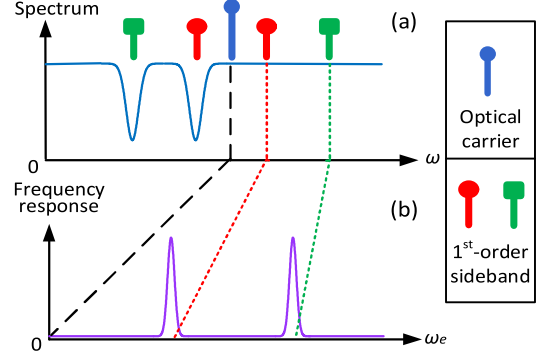


Fig. 4. Operation principle of the dual-passband MPF. (a) The transmission spectrum of the MDR and (b) the frequency response of the dual-passband MPF.

passbands are determined by the wavelength intervals between the optical carrier and two notches.

In the MDR, the central wavelengths of the two notches in the transmission spectrum can be expressed as

$$\lambda_{1,2} = \frac{2\pi n_{eff1,2} R}{m} \quad (1)$$

where  $n_{eff1,2}$  are the effective RIs of the first and third order WGM modes,  $R$  is the disk radius and  $m$  is the azimuth harmonic number of the WGM. The mode field of the TE modes decay rapidly outside the disk. Thus, when the disk surface environment varies,  $n_{eff1,2}$  will be changed, leading to the shifts of the resonance wavelengths. It is worth noting that  $n_{eff1,2}$  and the change rates of the different order modes are different, which leads to different wavelength shifts under the same environment variations. Assuming the wavelength and frequency of the optical carrier are  $\lambda_c$  and  $f_c$ , and the wavelength and frequency of the two notches representing the first and third order WGM mode resonances are  $\lambda_{1,2}$  and  $f_{1,2}$ , respectively, the central frequencies of the dual-passband MPF named  $f_{p1,p2}$  can be expressed as [20]

$$f_{p1,p2} = |f_{1,2} - f_c| = \frac{c|\lambda_c - \lambda_{1,2}|}{\lambda_c^2} \quad (2)$$

where  $c$  is the velocity of light in vacuum. When the MDR is experiencing temperature and/or RI variations, the wavelengths of the first and third order WGM mode resonances are shifted, given by [21], [22]

$$\Delta\lambda_{1,2} = \frac{\lambda_{1,2}}{n_g} \left[ \left( \alpha \cdot n_{eff1,2} + \frac{\partial n_{eff1,2}}{\partial T} \right) \Delta T + \left( \frac{\partial n_{eff1,2}}{\partial n_{sur}} \right) \Delta n_{sur} \right] \quad (3)$$

where  $n_g$  is the group index of the guided mode,  $\alpha$  is the coefficient of thermal expansion of the waveguide material,  $\Delta T$  is the temperature change,  $n_{sur}$  is the RI of the surroundings and  $\Delta n_{sur}$  is the surrounding RI change. According to (2) and (3), the central frequency changes of the two passbands of the dual-passband MPF, corresponding to the wavelength changes of the two notches in transmission spectrum of the MDR, produced by

temperature and RI variations are, respectively, given by

$$\begin{cases} \Delta f_1 = \frac{c}{\lambda_c^2} \cdot \Delta \lambda_1 = K_1^T \times \Delta T + K_1^n \times \Delta n_{sur} \\ \Delta f_2 = \frac{c}{\lambda_c^2} \cdot \Delta \lambda_2 = K_2^T \times \Delta T + K_2^n \times \Delta n_{sur} \end{cases} \quad (4)$$

As can be seen, both central frequencies of the two passbands of the MPF are linearly proportional to the temperature and RI variations with the sensitivities represented by  $K_{1,2}^{T,n}$ . By solving (4), temperature and RI measurements can be realized.

In the implementation, the central frequency changes are measured by applying a wideband LCMW to the MPF, to generate two filtered microwave waveforms. By measuring the temporal locations or equivalently central frequencies of the microwave waveforms, the frequency changes corresponding to the wavelength changes are measured. Owing to the high insert loss of the system, the filtered microwave waveforms are relatively weak with a poor SNR. Therefore, in the signal processing step, a noise reduction algorithm is introduced. A phase-only filter based on the input LCMW is built and is correlated with the filtered chirped microwave waveforms. The microwave waveforms are significantly compressed. However, since the distribution of the noise is random and is not correlated with the reference LCMW, the noise distribution is not altered. By applying a Hamming window to select the compressed waveforms, the noise is significantly suppressed. After re-correlating the noise-suppressed waveforms with the reference LCMW, the two microwave waveforms are recovered with a significantly improved SNR.

In the following, we show the SNR of the microwave waveforms can be improved. Assume the reference LCMW is  $r(t)$  and its Fourier transform is  $R(j\omega)$ . A phase-only filter is established by  $\frac{R^*(j\omega)}{|R(j\omega)|} = e^{j\phi_R(j\omega)}$ , where  $\phi_R(j\omega)$  is the phase term. A filtered chirped microwave waveform is given by

$$x(t) = s(t) + n(t) \quad (5)$$

where  $s(t)$  is the filtered chirped microwave waveform and  $n(t)$  is the noise. After correlation with the phase-only filter, we have a compressed waveform, given by

$$\begin{aligned} Y(t) &= F^{-1} \left[ X(j\omega) \times \frac{R^*(j\omega)}{|R(j\omega)|} \right] \\ &= F^{-1} \{ [S(j\omega) + N(j\omega)] \times e^{-j\phi_R(j\omega)} \} \\ &= F^{-1} [ |S(j\omega)| e^{j\phi_S(j\omega)} \times e^{-j\phi_R(j\omega)} + |N(j\omega)| e^{j\phi_N(j\omega)} \\ &\quad \times e^{-j\phi_R(j\omega)} ] \end{aligned} \quad (6)$$

where  $X(j\omega)$ ,  $S(j\omega)$  and  $N(j\omega)$  are the Fourier transforms of  $x(t)$ ,  $s(t)$  and  $n(t)$ , respectively,  $R^*(j\omega)$  is the complex conjugate of  $R(j\omega)$ , and  $\phi_S(j\omega)$ ,  $\phi_N(j\omega)$  and  $\phi_R(j\omega)$  are the phase terms of,  $S(j\omega)$ ,  $N(j\omega)$  and  $R(j\omega)$ , respectively. Since the filtered chirped microwave waveform is from the reference LCMW and the MPF has a linear phase response, the phase of the filtered chirped microwave waveform is same as

the reference LCMW. Thus, (6) is simplified as

$$\begin{aligned} Y_1(t) &= F^{-1} [ |S(j\omega)| e^{j\phi_R(j\omega)} \times e^{-j\phi_R(j\omega)} \\ &\quad + |N(j\omega)| e^{j\phi_N(j\omega)} e^{-j\phi_R(j\omega)} ] \\ &= F^{-1} [ |S(j\omega)| + |N(j\omega)| e^{j\phi_N(j\omega)} e^{-j\phi_R(j\omega)} ] \end{aligned} \quad (7)$$

Eq. (7) shows that a filtered microwave waveform is compressed. The phase of the noise is randomly distributed which means that the noise cannot be compressed and is still uniformly distributed.

By applying a Hamming window to extract the compressed waveform, the noise is suppressed significantly. Then, the recovered signal by re-correlating the compressed waveform with the phase-only filter can be written as

$$\begin{aligned} Y_2(t) &= F^{-1} [ (|S(j\omega)| + |N'(j\omega)| e^{j\phi_N(j\omega)} e^{-j\phi_R(j\omega)}) \\ &\quad \times \frac{R^*(j\omega)}{|R(j\omega)|} ] \\ &= F^{-1} [ |S(j\omega)| e^{-j\phi_R(j\omega)} \\ &\quad + |N'(j\omega)| e^{j\phi_N(j\omega)} e^{-j2\phi_R(j\omega)} ] \end{aligned} \quad (8)$$

where  $|N'(j\omega)|$  is the spectrum of the noise after windowing. As can be seen from (8), the microwave waveform after noise reduction processing is a time-reversed version of the microwave waveform, but the noise is significantly suppressed. Therefore, the filtered microwave waveform is rebuilt with an improved SNR.

### III. EXPERIMENTAL RESULTS

An experiment based on the setup in Fig. 1 is performed. A light wave generated by the LD (Yokogawa AQ2201) is directed to the 40-GHz PM (Throlabs), where the light wave is phase modulated by a chirped microwave waveform. The phase-modulated optical signal is sent via a grating coupler to the MDR where one sideband is suppressed. The optical signal at the output of the MDR is coupled out of the chip via a second grating coupler and amplified by the EDFA (Nortel FA17UFAC-119C28) before being applied to the 45-GHz PD (New Focus 1014), to recover the filtered microwave waveforms. The filtered microwave waveforms are sent to the DSP, where the SNR is improved and the central frequency changes are estimated. For temperature measurement, the MDR is immersed into pure water. The temperature is increased from 22.22 °C to 23 °C. Two filtered chirped microwave waveforms at five different temperatures are measured, as shown in Fig. 5(a). Due to the large optical insertion loss caused by low-coupling efficiency of the grating couplers and the low-power handling capability of the PD, the recovered chirped microwave waveforms have a relative low power, which makes the waveforms quite noisy. It is difficult to identify the central frequencies of the filtered chirped microwave waveforms directly. To improve the SNR of the waveforms, a noise reduction algorithm based on phase-only filtering and Hamming windowing is employed. Fig. 5(b) shows

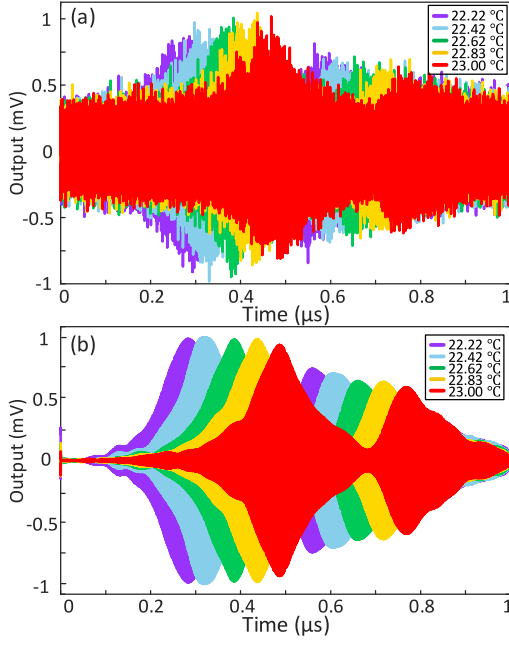


Fig. 5. The filtered chirped microwave waveforms with different temperatures (a) before the noise reduction and (b) after the noise reduction.

the waveforms after noise reduction. The noise is significantly suppressed and the SNR is significantly increased.

With the increase of the temperature, the central frequencies of two filtered chirped microwave waveforms are shifted to higher frequencies, due to the red shift of the two passbands of the MPF. By measuring the temporal locations or equivalently the central frequencies of the two filtered microwave waveforms, the wavelength changes of the two notches can be obtained. In this paper, we apply Fourier transform to the noise-reduced waveforms and measure the central frequencies.

Fig. 6(a) shows the spectra of the noise-reduced two filtered chirped microwave waveforms. The central frequencies of the two filtered chirped microwave waveforms are obtained by extracting the peak frequencies at different temperatures. Through plotting the experimental data with linear fitting, as shown in Fig. 6(b) and (c), the temperature sensitivities of the two chirped waveforms based on the WGM<sub>1,106</sub> and WGM<sub>3,96</sub> mode resonances are calculated, which are 8.2811 GHz/°C with a correlation coefficient ( $R^2$ ) of 0.9970 and 8.6884 GHz/°C with an  $R^2$  of 0.9961, respectively.

For RI sensing, the MDR is dripping with a saline solution having different RIs at a constant temperature. Fig. 7(a) shows the filtered chirped microwave waveforms with different RIs. Since the waveforms are very noisy, it is also difficult to directly measure the central frequencies. Again, we apply the noise reduction algorithm to the waveforms. As can be seen in Fig. 7(b), the noise is significantly reduced, and the SNR is increased. Two filtered chirped microwave waveforms shift to higher frequencies with the increase in the RI.

Fig. 8(a) shows the spectra of the noise-reduced two filtered chirped microwave waveforms. Through linear data fitting, as shown in Fig. 8(b) and (c), the RI sensitivities of the two filtered chirped waveforms based on the WGM<sub>1,106</sub> and

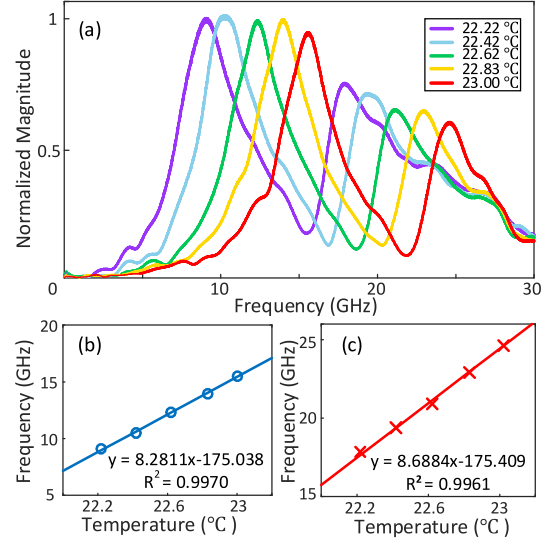


Fig. 6. (a) The spectra of the noise-reduced filtered chirped microwave waveforms with different temperatures; the relationships between the temperature and central frequencies of the noise-reduced filtered chirped microwave waveforms for (b) WGM<sub>1,106</sub> and (c) WGM<sub>3,96</sub> mode resonances.

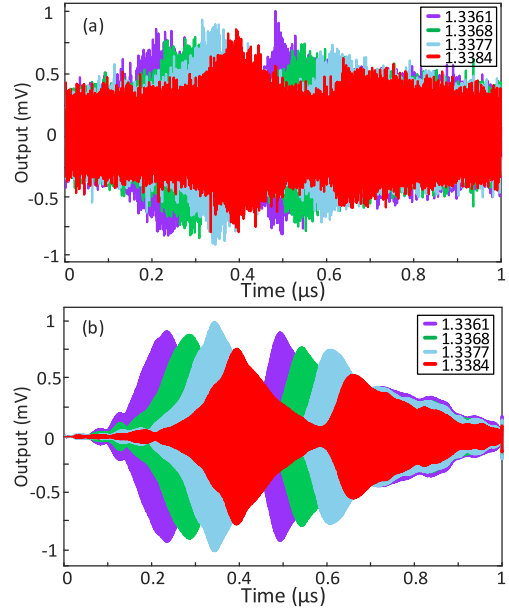


Fig. 7. The filtered chirped microwave waveforms with different RIs (a) before noise reduction and (b) after noise reduction.

WGM<sub>3,96</sub> mode resonances are calculated, which are 2195 GHz/RIU and 2344 GHz/RIU with  $R^2$ s of 0.9978 and 0.9999, respectively.

According to the experimental results, the relationship between the central frequencies of the two filtered chirped microwave waveforms and the changes in temperature and RI are given by

$$\begin{cases} \Delta f_1 = 8.2811 \times \Delta T + 2195 \times \Delta n_{sur} \\ \Delta f_2 = 8.6884 \times \Delta T + 2344 \times \Delta n_{sur} \end{cases} \quad (9)$$

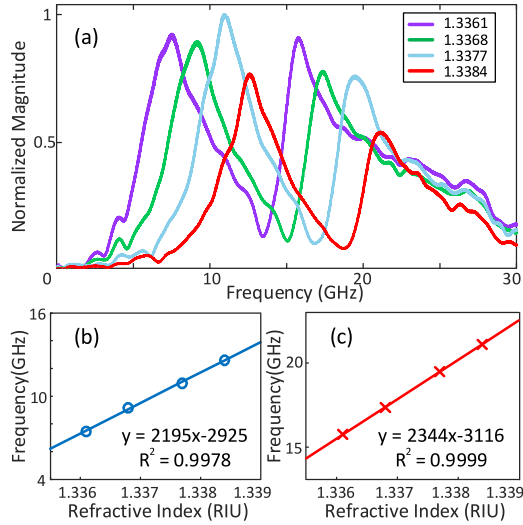


Fig. 8. (a) The spectrums of the noise-reduced filtered chirped microwave waveforms with different RIs; the relationships between the RI and central frequencies of the noise-reduced filtered chirped microwave waveforms for (b) WGM<sub>1,106</sub> and (c) WGM<sub>3,96</sub> mode resonances.

By measuring the central frequency changes, the temperature and RI changes can be calculated by

$$\begin{bmatrix} \Delta T \\ \Delta n_{sur} \end{bmatrix} = \begin{bmatrix} 6.8969 & -6.4585 \\ -0.0256 & 0.0244 \end{bmatrix} \begin{bmatrix} \Delta f_1 \\ \Delta f_2 \end{bmatrix} \quad (10)$$

Note that if the wavelength changes of the two notches are measured by an OSA with a resolution of 0.01 nm, the temperature and RI measurement resolutions are calculated to be 0.15 °C and  $5.7 \times 10^{-4}$  RIU, respectively. In the proposed interrogation approach, since the wavelength changes are converted to microwave waveform location changes in the time domain or microwave frequency changes, the frequencies can be accurately measured by a DSP. The resolution of the proposed system is thus limited by the sampling rate of the signal processor. In the experimental demonstration, an LCMW with a chirp rate of 32 GHz/ $\mu$ s was employed. The sampling rate of the oscilloscope used to perform signal digitization is 160 GSa/s. Thus, a minimum frequency measurement resolution is calculated to be 200 KHz or 1.6 fm. The temperature and RI measurement resolutions are  $2.4 \times 10^{-5}$  °C and  $9.1 \times 10^{-8}$  RIU, respectively, which are four orders of magnitude better than a conventional optical sensing system using an OSA. Note also that in the experiment, the broadband LCMW has a repetition rate of 1 MHz, thus the interrogation speed is 1 MHz. The speed can be higher if an LCMW with a higher repetition rate is employed.

#### IV. CONCLUSION

We have theoretically and experimentally investigated an on-chip integrated sensor based on a dual-passband MPF incorporating an integrated silicon photonic MDR for simultaneous RI and temperature measurements with high-speed and high-resolution interrogation. The key element in the system was an MDR which was used as a sensing element. Simultaneous temperature and RI sensing was achieved by measuring the wavelengths shifts of two notches of the MDR spectral response.

To increase the interrogation speed and resolution, the MDR was incorporated in an MPF to produce dual microwave passbands. By applying a broadband LCMW to the MPF, two chirped microwave waveforms with their temporal locations or equivalently central frequencies corresponding to the wavelength shifts of the notches were generated. To increase the SNR of the filtered microwave waveforms, a noise reduction algorithm based on phase-only filtering and Hamming windowing was proposed and employed. The proposed approach was experimentally evaluated. Simultaneous temperature and RI sensing with high interrogation resolutions of  $2.4 \times 10^{-5}$  °C and  $9.1 \times 10^{-8}$  RIU at a high interrogation speed of 1 MHz was demonstrated, which is four orders of magnitude higher than the use of an OSA.

#### REFERENCES

- [1] A. D. Kersey *et al.*, "Fiber grating sensors," *J. Lightw. Technol.*, vol. 15, no. 8, pp. 1442–1463, Aug. 1997.
- [2] A. Iadicicco, A. Cusano, A. Cutolo, R. Bernini, and M. Giordano, "Thinned fiber Bragg gratings as high sensitivity refractive index sensor," *IEEE Photon. Technol. Lett.*, vol. 16, no. 4, pp. 1149–1151, Apr. 2004.
- [3] A. Iadicicco, S. Campopiano, A. Cutolo, M. Giordano, and A. Cusano, "Refractive index sensor based on microstructured fiber Bragg grating," *IEEE Photon. Technol. Lett.*, vol. 17, no. 6, pp. 1250–1252, Jun. 2005.
- [4] W. Liang, Y. Huang, Y. Xu, R. K. Lee, and A. Yariv, "Highly sensitive fiber Bragg grating refractive index sensors," *Appl. Phys. Lett.*, vol. 86, no. 151122, pp. 1–3, Apr. 2005.
- [5] X. Fang, C. R. Liao, and D. N. Wang, "Femtosecond laser fabricated fiber Bragg grating in microfiber for refractive index sensing," *Opt. Lett.*, vol. 35, no. 7, pp. 1007–1009, Apr. 2010.
- [6] P. Prabhathan, V. M. Murukeshan, Z. Jing, and P. V. Ramana, "Compact SOI nanowire refractive index sensor using phase shifted Bragg grating," *Opt. Express*, vol. 17, no. 17, pp. 15330–15341, Aug. 2009.
- [7] J. Jágerská, H. Zhang, Z. Diao, N. L. Thomas, and R. Houdré, "Refractive index sensing with an air-slot photonic crystal nanocavity," *Opt. Lett.*, vol. 35, no. 15, pp. 2523–2525, Aug. 2010.
- [8] K. De Vos, I. Bartolozzi, E. Schacht, P. Bienstman, and R. Baets, "Silicon-insulator microring resonator for sensitive and label-free biosensing," *Opt. Express*, vol. 15, no. 12, pp. 7610–7615, Jun. 2007.
- [9] G. A. Rodriguez, S. Hu, and S. M. Weiss, "Porous silicon ring resonator for compact, high sensitivity biosensing applications," *Opt. Express*, vol. 23, no. 6, pp. 7111–7119, Mar. 2015.
- [10] V. M. N. Passaro, R. Loiacono, G. D'Amico, and F. De Leonardi, "Design of Bragg grating sensors based on sub micrometer optical rib waveguides in SOI," *IEEE Sensors J.*, vol. 8, no. 9, pp. 1603–1611, Sep. 2008.
- [11] J. Yao, "Microwave photonics for high resolution and high speed interrogation of fiber Bragg grating sensors," *Fiber Integr. Opt.*, vol. 34, no. 4, pp. 204–216, Oct. 2015.
- [12] H. Fu *et al.*, "High-frequency fiber Bragg grating sensing interrogation system using Sagnac-loop-based microwave photonic filtering," *IEEE Photon. Technol. Lett.*, vol. 21, no. 8, pp. 519–521, Apr. 2009.
- [13] W. Liu, M. Li, C. Wang, and J. Yao, "Real-time interrogation of a linearly chirped fiber Bragg grating sensor based on chirped pulse compression with improved resolution and signal-to-noise ratio," *J. Lightw. Technol.*, vol. 29, no. 9, pp. 1239–1247, May 2011.
- [14] J. Yao, "Photonic generation of microwave arbitrary waveforms," *Opt. Commun.*, vol. 284, no. 15, pp. 3723–3736, Jul. 2011.
- [15] F. Kong, W. Li, and J. Yao, "Transverse load sensing based on a dual-frequency optoelectronic oscillator," *Opt. Lett.*, vol. 38, no. 14, pp. 2611–2613, Jul. 2013.
- [16] H. Deng, W. Zhang, and J. P. Yao, "High-speed and high-resolution interrogation of a silicon photonic microdisk sensor based on microwave photonic filtering," *J. Lightw. Technol.*, to be published.
- [17] L. Gao, J. Zhang, X. Chen, and J. Yao, "Microwave photonic filter with two independently tunable passbands using a phase modulator and an equivalent phase-shifted fiber Bragg grating," *IEEE Trans. Microw. Theory Techn.*, vol. 62, no. 2, pp. 380–387, Feb. 2014.
- [18] W. Zhang and J. Yao, "Silicon-based single-mode on-chip ultracompact microdisk resonators with standard silicon photonics foundry process," *J. Lightw. Technol.*, vol. 35, no. 20, pp. 4418–4424, Oct. 2017.

- [19] J. Yao, "Optoelectronic oscillators for high speed and high resolution optical sensing," *J. Lightw. Technol.*, vol. 35, no. 16, pp. 3489–3497, Aug. 2017.
- [20] O. Xu, J. Zhang, H. Deng, and J. Yao, "Dual-frequency optoelectronic oscillator for thermal-insensitive interrogation of a FBG strain sensor," *IEEE Photon. Technol. Lett.*, vol. 29, no. 4, pp. 357–360, Feb. 2017.
- [21] J. J. Ackert *et al.*, "Defect-mediated resonance shift of silicon-on-insulator racetrack resonators," *Opt. Express*, vol. 19, no. 13, pp. 11969–11976, Jun. 2011.
- [22] G. D. Kim *et al.*, "Silicon photonic temperature sensor employing a ring resonator manufactured using a standard CMOS process," *Opt. Express*, vol. 18, no. 21, pp. 22215–22221, Oct. 2010.

**Jingxuan Liu** received the B.Eng. degree in automation from Beijing Jiaotong University, Beijing, China, in 2014. She is currently working toward the Ph.D. degree at the Key Laboratory of All Optical Network and Advanced Telecommunication Network, Ministry of Education, Institute of Lightwave Technology, Beijing Jiaotong University.

She is currently working as a joint training student with the Microwave Photonics Research Laboratory, School of Electrical Engineering and Computer Science, University of Ottawa, Ottawa, ON, Canada. Her current research interests include fiber optic sensors, optoelectronic oscillator, and silicon photonics application in sensing.

**Hong Deng** (S'16) received the B.Eng. degree in optoelectronic information engineering from the Huazhong University of Science and Technology, Wuhan, China, in 2014. He is currently working toward the Master's degree at the Microwave Photonics Research Laboratory, School of Electrical Engineering and Computer Science, University of Ottawa, Ottawa, ON, Canada.

His current research interests include photonic generation of microwave waveforms, fiber optic sensors, and silicon photonics.

**Weifeng Zhang** (S'12) received the B.Eng. degree in electronic science and technology from Xi'an Jiaotong University, Xi'an, China, in 2008, the M.A.Sc. degree in electrical engineering from the Politecnico di Torino, Torino, Italy, in 2011, and the Ph.D. degree in electrical engineering from the University of Ottawa, Ottawa, ON, Canada.

He is currently working as a Postdoctoral Fellow with the Microwave Photonics Research Laboratory, School of Electrical Engineering and Computer Science, University of Ottawa. His current research interests include silicon photonics and its applications in microwave photonics.

**Jianping Yao** (M'99–SM'01–F'12) received the Ph.D. degree in electrical engineering from the Université de Toulon et du Var, Toulon, France, in December 1997.

He is a Distinguished University Professor and a University Research Chair with the School of Electrical Engineering and Computer Science, University of Ottawa, Ottawa, ON, Canada. From 1998 to 2001, he was with the School of Electrical and Electronic Engineering, Nanyang Technological University, Singapore, as an Assistant Professor. In December 2001, he joined the School of Electrical Engineering and Computer Science, University of Ottawa, as an Assistant Professor, where he was promoted to an Associate Professor in May 2003, and a Full Professor in May 2006. He was appointed as the University Research Chair in Microwave Photonics in 2007. In June 2016, he was conferred the title of Distinguished University Professor of the University of Ottawa. From July 2007 to June 2010 and July 2013 to June 2016, he served as the Director of the Ottawa-Carleton Institute for Electrical and Computer Engineering. He has authored or coauthored more than 560 research papers including over 330 papers in peer-reviewed journals and more than 230 papers in conference proceedings.

Prof. Yao is the Editor-in-Chief of IEEE PHOTONICS TECHNOLOGY LETTERS, a Topical Editor of *Optics Letters*, an Associate Editor of *Science Bulletin*, a Steering Committee Member of IEEE JOURNAL OF LIGHTWAVE TECHNOLOGY, and an Advisory Editorial Board member of *Optics Communications*. He was a Guest Editor of a Focus Issue on Microwave Photonics in *Optics Express* in 2013, a Lead-Editor of a Feature Issue on Microwave Photonics in *Photonics Research* in 2014, and a Guest Editor of a special issue on Microwave Photonics in IEEE JOURNAL OF LIGHTWAVE TECHNOLOGY in 2018. He currently serves as the Chair of the IEEE Photonics Ottawa Chapter, and is the Technical Committee Chair of IEEE MTT-3 Microwave Photonics. He was a member of the European Research Council Consolidator Grant Panel in 2016, the Qualitative Evaluation Panel in 2017, and a member of the National Science Foundation Career Awards Panel in 2016. He has also served as a Chair of a number of international conferences, symposia, and workshops, including the Vice Technical Program Committee (TPC) Chair of the 2007 IEEE Topical Meeting on Microwave Photonics, TPC Co-Chair of the 2009 and 2010 Asia-Pacific Microwave Photonics Conference, TPC Chair of the high-speed and broadband wireless technologies subcommittee of the IEEE Radio Wireless Symposium 2009–2012, TPC Chair of the microwave photonics subcommittee of the IEEE Photonics Society Annual Meeting 2009, TPC Chair of the 2010 IEEE Topical Meeting on Microwave Photonics, General Co-Chair of the 2011 IEEE Topical Meeting on Microwave Photonics, TPC Co-Chair of the 2014 IEEE Topical Meetings on Microwave Photonics, and General Co-Chair of the 2015 and 2017 IEEE Topical Meeting on Microwave Photonics. He has also served as a committee member for a number of international conferences, such as IPC, OFC, BGPP, and MWP. He was the recipient of the 2005 International Creative Research Award of the University of Ottawa, the 2007 George S. Glinski Award for Excellence in Research, and the Natural Sciences and Engineering Research Council of Canada Discovery Accelerator Supplements Award in 2008. He was selected to receive an inaugural OSA Outstanding Reviewer Award in 2012 and was one of the top ten reviewers of IEEE/OSA Journal of Lightwave Technology 2015–2016. He was an IEEE MTT-S Distinguished Microwave Lecturer for 2013–2015. He was the recipient of the Award for Excellence in Research 2017–2018 of the University of Ottawa. He is a registered Professional Engineer of Ontario. He is a Fellow of the Optical Society of America, the Canadian Academy of Engineering, and the Royal Society of Canada.